Localized Corrosion Risk Assessment Using Markov Analysis

K. McCallum, J. Zhao,* M. Workman,* M. Iannuzzi,** M. Kappes,*** J. Payer,**** C.B. Clemons,* S. Chawla,***** K.I. Kreider,* N. Mimoto,****** and G.W. Young‡,**

ABSTRACT

The objective of this work was to develop the foundation for an interactive corrosion risk management tool for assessing the probability of failure of equipment/infrastructure as a function of threats (such as pitting corrosion and coating degradation) and mitigation schemes (such as inhibitors and coatings). The application of this work was to assist with corrosion management and maintenance planning of equipment/infrastructure given dynamic changes in environmental conditions. Markov models are developed to estimate pitting damage accumulation density distributions as a function of input parameters for pit nucleation and growth rates. The input parameters are selected based upon characterization with experimental or field observations over a sufficiently long period of time. Model predictions are benchmarked against laboratory pitting corrosion tests and long-term atmospheric exposure data for aluminum alloys, obtained from the literature. The models are also used to examine hypothetical scenarios for the probability of failure in pipeline systems subject to sudden, gradual, and episodic events that change the corrosive conditions.

KEY WORDS: corrosion, Markov, model, Monte Carlo, pitting damage

INTRODUCTION

The objective of this work was to formulate the basic methodology for a probabilistic analysis tool to assist with corrosion risk management of equipment/infrastructure that is subject to dynamic corrosive degradation processes and mitigation schemes. We illustrate the use of the tool for analyzing two contrasting cases:

—pitting corrosion risk assessment of high-strength aluminum alloys
—leak probability as a result of pitting corrosion in a carbon steel pipe

Risk assessment, for example, in aging airplanes, involves estimating the size of pits that can act as initiation sites for corrosion fatigue cracks. We formulate the foundation for a predictive methodology to estimate pit depth size distribution in high-strength aluminum alloys, such as AA7075 (UNS A97075)[1] and AA2024 (UNS A92024), used in aerospace applications. The predictive methodology is also applied to an oil pipeline subject to internal pitting corrosion, and examines the corrosive behavior for various pipeline corrosion scenarios. The methodology may be extended to equipment and infrastructure made from other materials for prediction of the reliability and useful lifetime of the equipment/infrastructure, given dynamic changes in its operating conditions.

Submitted for publication: November 5, 2013. Revised and accepted: April 29, 2014. Preprint available online: May 22, 2014, doi: http://dx.doi.org/10.5006/1184.
‡ Corresponding author. E-mail: gyoung1@uakron.edu.
* The University of Akron, Department of Mathematics, Akron, OH 44325-4002.
** The University of Akron, Department of Chemical and Biomolecular Engineering, Akron, OH 44325-3906. Currently at General Electric—Oil and Gas, NO-1338 Sandvika, Norway.
*** The University of Akron, Department of Chemical and Biomolecular Engineering, Akron, OH 44325-3906.
**** The University of Akron, Corrosion and Reliability Engineering, Akron, OH 44325-9006.
***** Det Norske Veritas (USA), Inc., Dublin, OH 43017.
****** The University of Akron, Department of Statistics, Akron, OH 44325-1913.
[1] UNS numbers are listed in *Metals and Alloys in the Unified Numbering System*, published by the Society of Automotive Engineers (SAE International) and cosponsored by ASTM International.

ISSN 0010-9312 (print), 1938-159X (online)
14/0000181/$5.00+$0.50/0

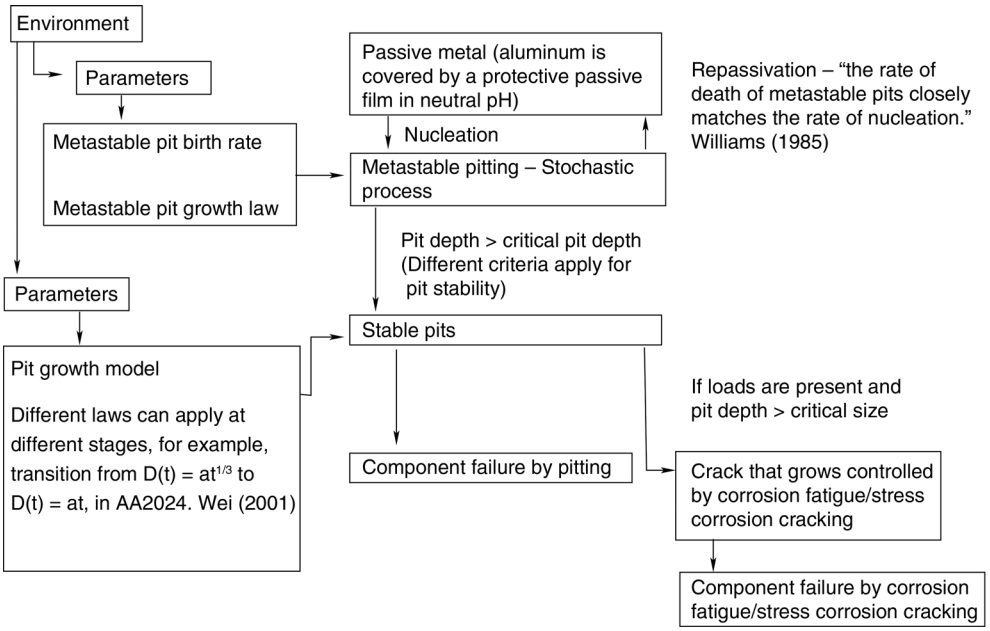

FIGURE 1. *Overview of stages of damage accumulation in aluminum alloys (Wei[1] and Williams, et al.[2-3]).*

MODEL DEVELOPMENT

Figure 1 illustrates the main processes in pitting corrosion (right column) and the inputs (left column) needed by models to simulate the processes.[1-3] Models require a pit birth rate and growth rate. Ideally, both rates should be functions of the metal-environmental conditions. Both metastable and stable pits should be simulated. This study only considers stable pits that have reached a critical depth that will sustain pit growth.[4] Future work will consider modifications to the proposed models to include metastable pits and repassivation.

Markov analysis is used to define a methodology for simulating pitting corrosion. Both Markov chain process (MCP) solution procedures and Monte Carlo (MC) simulations are conducted. The first step of the Markov model is to predict the number of pits that initiate on a sample specimen, as well as their initiation times in a given time window. Based upon literature data sets[5-7] of pit density as a function of time, we pose an expression for the average number of pits over a reference area in a nonhomogeneous Poisson model for pit initiation. Once a pit is initiated, the Markov model is used to determine the propagation of pit depth over time. Expressions for the pit growth rate are based on general power laws, discussed in the literature.[8] Such laws attempt to describe pit growth behavior as a function of ohmic effects, charge transfer, mass transport, corrosive conditions, materials, flow rates, type of the flowing substance (gas, oil, water), etc., or a combination of these effects. In particular for high-strength aluminum alloys, it has been suggested that pit growth can be controlled by the rate of cathodic reactions occurring in intermetallic particles.[9-11] Several of the different pit growth laws may be embedded in the pit growth rate expression to capture time-dependent transitions in the growth process. Hence, the flow of the Markov process is straightforward and consistent with the temporal flow of the physical processes in pit initiation and growth.

Using a Markov chain process,[12-19] we formulate differential equations for probability distributions of a population of pits being in a defined set of corroded states. Each state represents a specific pit depth. Pit growth is assumed to occur in discrete jumps from an array of n possible states. The transition rates between states are based upon the general power laws, discussed above. By adjusting these transition rates between states, we represent the dynamic corrosive and mitigation conditions to which the metal is subjected. The transition rate models used here are flexible and capable of accommodating a wide range of corrosive and mitigation scenarios.

This nonhomogeneous Markov chain model for pit growth is combined with the nonhomogeneous Poisson model for pit initiation. The result is an expression for the cumulative distribution function (CDF), which defines the probability that the maximum pit depth is less than or equal to state i.

Once the CDF is determined either by MCP or MC, the probability mass function for each state (pit depth) is calculated along with mean maximum pit depth and variance over time. Both MCP and MC calculations for pit size distribution are benchmarked against real pit depth data sets, representing short-time laboratory and long-term atmospheric corrosion scenarios, obtained by profilometery and

TABLE 1
Model Parameters and Outputs

Variable	Description	Equation Number
A, μ, ν, β	Parameters for the number of pits	(1)
u	Time at which a pit nucleates	(5)
D(t)	Pit depth	(5)
b	Power law exponent for pit depth	(5)
C	Discretized metal thickness	(5)
i	State of pit depth	(5)
λ_i	Transition rate between states	(6),(8)
$P_i(t)$	Probability of being in state i	(3),(9)
$\theta_i(t)$	Cumulative distribution function for the probability that the maximum pit depth is less than or equal to state i	(12),(18),(19)

optical microscopy.[5,12-13] To illustrate the flexibility of the approach, the models are also used to examine hypothetical scenarios for the probability of failure in pipeline systems subject to sudden, gradual, and episodic events that change the corrosive conditions. For the model development that follows and for later reference, we summarize key model parameters and outputs in Table 1.

Pit Initiation Model

For a metal surface, we assume the surface has been tessellated into an appropriate grid. Each local section of the grid is characterized by its own pit density (number of pits per area) distribution. We focus on a single section of interest on the metal surface. Based upon experimental data plots of pit density vs. time (see References 2 and 3 for several examples), it appears that pit density increases in time according to profiles that vary from exponential to linear distributions over time. It is our general observation that pit density initially increases over time, reaches a maximum, and then may decrease as a result of pit coalescence.[5,11] Hence, we assume the average number of pits, measured over a reference area in the section of interest, over time is modeled as:

$$APD(t) = \frac{A}{\mu}\left[1 - e^{-\mu t}\right] + \nu t^{B} \qquad (1)$$

Here, the parameters A, μ, ν, and β will generally be constants, though it is conceivable that they could depend upon time. The latter case allows for the possibility that pit initiation rates can transition as a result of changing environmental conditions.

Using Equation (1), we define the probability that the average number of pits, N(t), at time t is m pits by a nonhomogeneous Poisson initiation process:

$$\Pr\left[N(t) = m\right] = \frac{1}{m!}\left[APD(t)\right]^{m} e^{-APD(t)} \qquad (2)$$

This process is chosen for two reasons:

—The Poisson process is the simplest distribution used to simulate the initiation of discrete events.
—The mean value for the Poisson distribution as defined in Equation (2) is APD(t).

Hence, we establish Equation (1) as the average number of pits over time for the proposed nonhomogeneous Poisson initiation process. The latter reason plays a critical role in the solution procedure that follows. Through various assumptions in the solution procedure, ultimately, we shall only need the expected value of the probability distribution for the average number of pits.

We note that our proposed pit initiation model differs from others in the literature. In particular, we recognize the extensive work by Caleyo and Valor[15-16,20] in the area of developing combined pit initiation/pit growth models using Markov analysis. Those investigations used a Weibull distribution for the pit initiation. Both their proposed distribution and ours requires the selection of fitting parameters to establish the increase in the number of pits over time. These parameters can be chosen based upon a match with measured data sets of pit density, or to simulate hypothetical pit initiation rates. An advantage of the proposed pit initiation model over the Weibull distribution is that choosing the fitting parameters in Equation (1) is more intuitive. For example, to simulate a situation where the number of pits increases linearly with time, one sets A = 0 and β = 1.

Finally, we acknowledge the pit initiation model comprehensively developed by the Hudson and Scully group.[21-26] Their model is based upon a transition to pitting corrosion from the spatiotemporal interactions of metastable pits that lead to a single metastable pitting event autocatalytically enhancing the probability of subsequent events. The spatial effects are accounted for through local changes in aggressive species concentration, potential drop, and oxide film damage. The result is an event generation rate based upon a combination of measurable environmental factors and some fitting parameters. Spatial and environmental factors are missing from the proposed equation for APD(t). These are to be included in the next iteration of our pit initiation model.

Pit Growth Model

To establish a pit growth model for a population of pits, we closely follow the work of Valor and coworkers.[15-16,20] Where appropriate, we highlight the differences between our approach and theirs. The Markov chain process concept for pit growth is to discretize the metal thickness into n states of equal thickness C. The continuous pit depth D(t) is replaced by this discrete set of states, where D(t) ~ C(i − 1) with i denoting a particular state, i = 1, 2, . . . , n+1. State 1 corresponds to the uncorroded metal. State 2 describes pits of depth C, and the final state n + 1 represents failure. Here, failure is defined as through

thickness pit penetration. Let $P_i(t)$ be the probability of pit depth being in state i at time t, and $\lambda_i(t)$ be the probabilistic transition rate to move from state i to state i + 1. The transition rate may be related to the pit growth rate.[20,27] In this study we examine general models for $\lambda_i(t)$ and a specific model for $\lambda_i(t)$ with the mathematical structure $\lambda_i(t) = \alpha(t)i$. For all cases, we only consider stable pit growth. We have neglected the possibility of metastable pits that may repassivate immediately after nucleation, or grow for a short time and then repassivate. It has been shown that separate pit depth models may be required to distinguish stable pit depth distributions from metastable distributions.[28-29] We note that the Monte Carlo model developed by Murer and Buchheit[27] includes both stable and metastable pits.

Under the above definitions, the overall MCP is governed by a system of ordinary differential equations defining the transition from state to state:

$$\begin{aligned} \frac{dP_1(t)}{dt} &= -\lambda_1(t)P_1(t) \\ \frac{dP_i(t)}{dt} &= -\lambda_i(t)P_i(t) + \lambda_{i-1}(t)P_{i-1}(t), \text{ for } i = 2,3,\ldots,n \end{aligned} \tag{3}$$

The probability of being in state n + 1 is $P_{n+1}(t) = 1 - \Sigma_{i=1}^{n} P_i(t)$. This system of equations is subject to the initial probability distribution of pit depths being in each state. For example, if the metal begins in an uncorroded state, then $P_1(0) = 1$ and $P_i(0) = 0$, i = 2, 3,..., n + 1. Here, one can follow the corrosion of a population of pits and predict the probability distribution of the pits being at a certain depth over time. In another scenario, the metal of interest, say the aluminum skin of a plane, may initially be in an arid environment. Pits develop under this condition. If the plane is then stationed in a more tropical environment, the initial pit depth distribution in the tropical environment is taken as the final distribution from the arid environment. The pit transition rates are adjusted for the tropical environment to predict the future probability distribution of pit depth. As shown below, for a given environment, the depth distribution of multiple pits will be modeled. Further, we will show how environmental history is captured via fitting parameters that define the transition rates $\lambda_i(t)$.

Next, we propose two models for the transition rate $\lambda_i(t)$ from state to state. We provide a description for the motivation behind the proposed rates. However, the ultimate justification for the proposed transition rates will be showing that the results we obtain for pit depth distribution over time, using these rates, are consistent with experimental and field observations.

To motivate the models for transition rate, we begin with an accepted power law model[8] for the pit depth, $D(t) = a(t - u)^b$, where u is the time at which a pit initiates, and a and b are parameters defining the rate of the pit growth. Generally, a and b are constants. However, these may be functions of time to account for changing environmental conditions and/or materials microstructure.[11] Allowing these to change with time keeps the mathematical format of the power law. Given the definitions of the discrete thickness C of the metal layers and the transition rate $\lambda_i(t)$, there are continuous and discrete expressions for the pit propagation rate that we assume are approximately equivalent:

$$\frac{\frac{dD}{dt}}{C} \approx \frac{di}{dt} \approx \lambda_i \tag{4}$$

In the above, the first expression represents the continuous rate at which the pit depth propagates from state to state. This is approximately equal to the second expression for the discrete rate of moving from state to state, which is then connected to the transition rate $\lambda_i(t)$ from state to state. Integration of Equation (4) leads to approximate equivalencies between continuous and discrete expressions for the pit depth:

$$D(t) = a(t)(t - u)^{b(t)} \approx C(i - 1) \approx C\int_u^t \lambda_{i-1}(\tau)\,d\tau \tag{5}$$

Using these expressions and approximating C by $\frac{D(t)}{i-1}$, we obtain:

$$\begin{aligned} \lambda_{i-1} &= \frac{\frac{dD}{dt}}{D}(i - 1) = \\ &\left[\frac{b(t)}{t - u} + \frac{a'(t)}{a(t)} + b'(t)\ln(t - u)\right](i - 1) = \alpha(t)(i - 1) \end{aligned} \tag{6}$$

Solving the relationship $a(t)(t - u)^{b(t)} \approx C(i - 1)$ in Equation (5) for t – u, and then substituting this expression for t – u into Equation (6):

$$\lambda_{i-1} = \left(\frac{b(t)\left(\frac{C}{a(t)}\right)^{-1/b(t)}}{(i-1)^{1/b(t)}} + \frac{a'(t)}{a(t)} + \frac{b'(t)}{b(t)}\left[\ln\left(\frac{C}{a(t)}\right) + \ln(i-1)\right]\right)(i - 1) \tag{7}$$

where $0 < b < 1$. In cases where a and b are constants or a′ and b′ are sufficiently small in magnitude, this can be simplified to:

$$\lambda_{i-1} = \frac{b\left(\frac{C}{a}\right)^{-1/b}}{(i-1)^{1/b}}(i - 1), \quad i = 2,3,\ldots,n+1 \tag{8}$$

Therefore, we have provided motivation for two expressions for λ_i. In Equation (6), λ_i fits the format $\lambda_i = \alpha(t)i$, where $\alpha(t)$ is the expression in brackets. The other transition rate expression for λ_i, given by Equa-

tion (8), does not fit this format. It is important to distinguish whether or not the expression for λ_i fits the format $\lambda_i = \alpha(t)i$, because under this format the MCP Equation (3) can be solved analytically.[30] Outside this format, one must solve the equations numerically. Since we have proposed two transition rates, one that fits the format and one that does not, we outline the solution of the MCP Equation (3) for each scenario.

For the case $\lambda_i = \alpha(t)i$, we restrict to the initial conditions $P_1(u) = 1$ and $P_i(u) = 0$, i = 2, 3,..., n + 1 for pits that initiate at time u. Hence, the analytical solution for Equation (3) becomes:[30]

$$P_i(t) = \exp[-\rho(t)](1 - \exp[-\rho(t)])^{i-1} \quad (9)$$

where:

$$\rho(t) = \int_u^t \alpha(\tau)\, d\tau = \ln[D(t)] - \ln[D(u)] \quad (10)$$

In the latter expression, we have used $\frac{\frac{dD}{dt}}{D} = \alpha(t)$ from Equation (6).

Equation (10) illustrates the singularity associated with the $\frac{b}{t-u}$ term in the expression for α since D(u) = 0. To alleviate this singularity we adjust the singular term to the form $\frac{b}{t-u+\epsilon}$ where ϵ is small. We note that for other initial conditions an analytical solution also exists.[20] In the case that $P_1(u) = 0$, the singularity does not exist because the pits are assumed to have some finite depth at the onset so that $D(u) \neq 0$.

Analytical solutions are not available when λ_i does not follow the $\lambda_i = \alpha i$ format. Here, we present results obtained either through numerical solutions of the governing differential Equation (3) or through MC simulations. The numerical approach is also benchmarked against the analytical solutions for the $\lambda_i = \alpha i$ scenario.

In summary, this study uses a single Markov growth model with both the ϵ-adjusted Equation (6) for λ_i together with the analytical solution (Equation [9]), as well as the Equation (8) for λ_i with numerical simulations of system (Equation [3]) or MC to simulate pit growth scenarios. The former expression for λ_i allows for the use of the analytical solutions that are restricted to the $\lambda_i = \alpha i$ model. The use of Equation (6) differs from other investigations,[20] where Equation (10) is used only for $P_1(u) = 0$ scenarios, while $\rho = D(t)$ is used when $P_1(u) = 1$. Given the logarithmic expression for ρ, a value for parameter a in the definition $D(t) = a(t-u)^b$ is not needed. Hence, the only input to the MCP model is an expression for b. This expression may either be a constant, representing constant corrosive conditions, or a function of time to simulate changing corrosive conditions. In this situation, expressions for the probabilities $P_i(t)$ will be calculated using the analytical expression in Equation (9). However, Equation (8) allows for more complicated structures for λ_i that may be used to simulate repassivation or other growth situations where transitions from state to state depend strongly on depth. Here, numerical simulations are conducted.

Combined Pit Initiation/Pit Growth Model

Next, we develop the combined pit initiation/pit growth model. Given that m pits are generated in (0, t) at times u_j, for j = 1,...m, then the cumulative distribution function, $\theta_i(t)$, for the probability that the maximum pit depth is less than or equal to state i is:

$$\theta_i(t) = \sum_{m=0}^{\infty} (\text{probability that m pits per area have initiated by time t}) \times (\text{probability that each pit is in a state less than or equal to i, given that there are m pits that have initiated}) \quad (11)$$

The former probability is defined in Equation (2). The latter probability is established in steps by first determining the probability, $F(t, i; u_j)$, that a pit is in a state less than or equal to i. Given the probability, $P_k(t; u_j)$, of a pit being in a certain depth state, defined by the solution of Equation (3), we have $F(t, i; u_j) = \sum_{k=1}^{i} P_k(t; u_j)$. Since $F(t, i; u_j)$ depends upon the initiation time u_j, then one must account for all possible distributions of initiation times. For this purpose, we introduce the joint density of initiation times given m pits, $f(u_1, u_2, \ldots, u_m | N(t) = m)$. We do not provide an explicit form for $f(u_1, u_2, \ldots, u_m | N(t) = m)$, because this is not needed in the solution procedures outlined below. Nevertheless, using these definitions of the probabilities in Equation (11), we do define the general expression for the cumulative distribution function, $\theta_i(t)$, for the probability that the maximum pit depth is less than or equal to state i as:

$$\theta_i(t) = \sum_{m=0}^{\infty} \Pr[N(t) = m] \int_0^t \int_0^{u_{m-1}} \cdots \int_0^{u_2} \prod_{j=1}^{m} F(t, i; u_j)\, f\, du_1 \cdots du_m \quad (12)$$

Because of its complexity, Equation (12) is not used in this most general form to calculate $\theta_i(t)$. Rather, we first use the kinetic Monte Carlo method, as described next, to compute the complete Equation (12) without approximation and without an explicit form for $f(u_1, u_2, \ldots, u_m | N(t) = m)$. Once the Monte Carlo simulations are complete, we provide an approximate expression for Equation (12) in Equation (19) that follows. This approximate expression is used with the Markov chain approach to also calculate $\theta_i(t)$. These calculations with the approximate expression are significantly faster, seconds vs. hours, than the Monte Carlo simulations. The Monte Carlo and Markov chain results are compared to justify the use of the approximate expression for Equation (12).

Monte Carlo Simulations — To compute Equation (12) without any conceptual approximation, we use

the kinetic Monte Carlo method described in Prados, et al.[31] The kinetic Monte Carlo method allows us to simulate the development of the pits chronologically. Pits are initiated stochastically according to our nonhomogeneous Poisson process at a rate derived from Equation (1). As new pits initiate, each existing pit grows stochastically according to the Markov model with transition rate, $\lambda_i(t)$. There are no requirements on the analytical form of $\lambda_i(t)$.

Specifically, in the MC method, we first derive the probability distribution of waiting times for pit initiation. It is well known that if the Poisson process were homogeneous and characterized by a constant rate of c events per unit time, then the waiting time between events is exponentially distributed with mean 1/c. For our case, the nonhomogeneous Poisson process is characterized by the time-dependent mean Equation (1). Hence, we define the number of pits initiated per area in the time interval (t_1, t_2) as:

$$g(t_1, t_2) = \frac{A}{\mu}\left[e^{-\mu t_1} - e^{-\mu t_2}\right] + \nu\left(t_2^{\beta} - t_1^{\beta}\right) \quad (13)$$

Note that APD(t) = g(0, t). Define the waiting time, γ_t, to be the time from t to the next pit initiation. Then, the cumulative distribution function (CDFW) of the waiting times can be written as:[32]

$$F_{\gamma t}(\chi; t) = P(\gamma_t \le \chi) = 1 - e^{-g(0,t+\chi)} - \int_0^t \frac{d}{dy} g(0, y) e^{-g(y,t+\chi)} dy \quad (14)$$

In the Monte Carlo simulation, pits are initiated as follows. The first pit initiation time, u_1, is a random sample from the CDFW $F_{\gamma t}(x; 0)$. The second initiation time, u_2, is a random sample from the CDFW $F_{\gamma t}(x; u_1)$. One continues in this fashion until the predetermined stopping time, t_{stop}, is reached. The result is a set of simulated initiation times $u_1, \ldots, u_m < t_{stop}$, which follow the nonhomogeneous Poisson process with the time-dependent mean Equation (1). Note that for a fixed value of t_{stop}, the number, m, of initiated pits is random and different for each simulation iteration. The expected value of m is $E(m) = APD(t_{stop})$.

Next, each of the initiated pits grows stochastically in depth according to the Markov model with transition rate, $\lambda_i(t)$, according to the algorithm developed by Prados, et al.[31] We define the residence time of the jth pit, $\tau_i^{(j)}$, to be the time the jth pit spends in state i. The simulation of pit growth is performed as follows. All the initiated pits start in state 1. For the first pit, initiated at time u_1, the algorithm generates $\tau_1^{(1)}$ by numerically determining $\tau_1^{(1)}$, such that:

$$-\log U = \int_{u_1}^{u_1+\tau_1^{(1)}} \lambda_1(\chi) d\chi \quad (15)$$

where U is a random sample from the uniform(0,1) distribution. This means that the first pit grows from state 1 to state 2 in the time $t = u_1 + \tau_1^{(1)}$. Then $\tau_2^{(1)}$ is generated using:

$$-\log U = \int_{u_1+\tau_1^{(1)}}^{u_1+\tau_1^{(1)}+\tau_2^{(1)}} \lambda_2(\chi) d\chi \quad (16)$$

where U is a random sample from the uniform (0,1). One repeats this process for $\tau_3^{(1)}, \tau_4^{(1)}, \ldots$ until t_{stop} is exceeded. Simulation then moves on to the growth of the second initiated pit (initiated at u_2), generating $\tau_1^{(2)}, \tau_2^{(2)}, \ldots$ until t_{stop} is exceeded. This process repeats for all initiated pits.

At the completion of one iteration, which includes the initiation and growth stages for each pit, the simulation has generated $\{u_j, \tau_1^{(j)}, \ldots, \tau_{kj}^{(j)}\}$ for the jth pit $(1 \le j \le m)$. Note that k_j is the maximum state reached by the jth pit before t_{stop}, and is different for each pit. Therefore, for each pit, one determines $S_j(t)$, the state of the jth pit at time t, $0 < t \le t_{stop}$. For this single iteration, the maximum pit depth at time t can be calculated as $MPD(t) = \max(S_1[t], \ldots, S_m[t])$.

Repeat the iteration process and let $MPD_l(t)$ be the maximum pit depth at time t, generated by the lth iteration. This simulation scheme is iterated 1,000 times, recording the pit initiation times and growth paths for each pit. We compute the empirical cumulative probability that the maximum pit depth is less than or equal to state i by determining the proportion of $MPD_l(t)$ values below i as

$$\hat{\theta}_i(t) = \frac{\sum_{l=1}^{1,000} I(MPD_l[t] \le i)}{1,000} \quad (17)$$

where I denotes the indicator function, whose value is 1 if the inequality is true. It is known[31] that the empirical distribution function $\hat{\theta}_i(t)$ converges to $\theta_i(t)$, defined in Equation (12), for all t, as the number of iterations approaches infinity.

A drawback of the MC simulation is the computation time. Typically, the computations, outlined above, require several hours. Hence, in the next section, we propose a simplification scheme—Equation (19) for the cumulative distribution function, $\theta_i(t)$—that reduces the computation time to seconds. The results from Equation (17) are compared with results from Equation (19) to justify the use of the approximate Equation (19).

Simplification Schemes for the Cumulative Distribution Function, $\theta_i(t)$ — Because of its complexity, several simplification schemes have been used for the computation of $\theta_i(t)$ as defined in Equation (12). First, Hong[15] used an MCP model where λ_i was assumed to be the same constant for all i. Under this scenario, Equation (12) was reduced analytically to:

$$\theta_i(t) \approx \sum_{m=0}^{\infty} Pr[N(t) = m]\left(\frac{1}{t}\int_0^t F(i, t; u)\, du\right)^m \quad (18)$$

The expression $\frac{1}{t}\int_0^t F(i, t; u)du$ can be interpreted as a replacement for the iterated integrals in Equation (12). This replacement is the expected value of the probability that the pits are in a state less than or equal to i, regardless of the initiation times of the pits. Here, the probability that each of the m pits is in a state less than or equal to i is identical for each pit. We do not use Equation (18) in the calculations that follow. Rather, we use a different simplification scheme that is outlined next.

Our proposed simplification scheme for Equation (12) also replaces the iterated integrals in Equation (12) by mean value expressions. Further, the pit initiation process, defined by Equation (2), is replaced by its mean, Equation (1). In other words, the pits are now initiated deterministically according to Equation (1). This conceptual simplification significantly reduces the complexity of Equation (12). Therefore, the cumulative probability that the maximum pit depth is less than or equal to state i is:

$$\theta_i(t) \approx \sum_{m=0}^{\infty} \Pr[N(t) = m]\left(\prod_{j=1}^{m} F(i, t; E(u_j))\right) \approx \prod_{j=1}^{\text{Floor}_{[E(N(t))]}} F(i, t; E(u_j)) \quad (19)$$

Here $E(\cdot)$ denotes the expected value of the expression, and the floor function is used to obtain an integer value for the number of pits. Hence, from Equations (1) and (2), we have $E(N[t]) = APD(t)$. Further, the expected time, $E(u_j)$, for the initiation of the jth pit is determined as the solution of the algebraic equation $APD(E[u_j]) = j$.

The advantage we gain by using Equation (19) is that the computation time is reduced to seconds, even when conducting numerical simulations of Equations (3) for $P_k(t; u_j)$. In the "Discussion" section, we demonstrate the numerical equivalence between results obtained through MC simulations using Equation (17), and those obtained through MCP computations using Equation (19). Equation (19) for the cumulative probability distribution will be used in the MCP solution procedure for the remainder of this study.

Statistics of the Pit Depth Distribution

Regardless of the approach used to calculate $\theta_i(t)$, we use $\theta_i(t)$ to calculate the frequency distribution of pit depth. The probability mass function, PMF, for state i is given by:

$$PMF(i, t) = \theta_i - \theta_{i-1} \quad (20)$$

Hence, one can now calculate the state at which the mean maximum pit depth (MMPD) occurs:

$$MMPD(t) = \sum_{i=1}^{n} i \times PMF(i, t) \quad (21)$$

and the variance:

$$\sigma^2(t) = \sum_{i=1}^{n} i^2 \times PMF(i, t) - [MMPD(t)]^2 \quad (22)$$

Predictions for the mean maximum pit depth and variance, using the above expressions multiplied by the width C of the states, will be presented in the results section to follow.

RESULTS AND DISCUSSION

Benchmark the Model Against Short-Term Laboratory Data

We present the use of the combined pit initiation/pit growth model to simulate pit initiation and the mean maximum pit depth for pitting corrosion in steel coupons placed in water, according to the experiments conducted by Rodriquez and Provan.[12-13] This data set has been studied several times in the literature[15-16] and so allows us to benchmark our approach against the other investigations. In those previous investigations and in ours, one must first set the number of states in the Markov model. We elaborate on the influence of the number of states later in this manuscript, and for now select 100 states, consistent with previous investigations. Hong[15] uses a constant value for λ together with Equation (1) (A = 0) for the number of pits. Valor, et al.,[16] use $\rho = D(t)$ and a Weibull distribution for the number of pits. We use the ϵ-adjusted Equation (6) for λ and Equation (2) for the number of pits. All three approaches select model parameters through curve fits to the mean maximum pit depth data in Rodriquez and Provan.[12-13] As discussed in Valor, et al.,[16] their approach provides excellent agreement to both the mean maximum pit depth and variance data, while Hong's approach matches to the mean maximum pit depth, but does not match well with the variance.

Figure 2 shows a comparison of the mean maximum pit depth and variance computed by our MCP procedure (b = 0.09172, ϵ = 0.001562, ν = 0, A = 1,590,000, and μ = 1,000) with the Rodriquez and Provan data. Similar to Valor, et al., we too obtain excellent agreement with both the mean maximum pit depth and the variance because the parameters of the model were chosen to fit the data. Further, our predictions for the number of pits also agree with Valor, et al., with both models predicting development of 1,590 pits per area in less than one day. We comment that our approach for this data set uses $\lambda = \frac{b}{t - u + \epsilon}$. Rodriquez and Provan use the somewhat similar expression $\lambda = \frac{\gamma(1 + \gamma t)}{1 + \gamma t^{\kappa}}$ and obtain excellent agreement to both the mean maximum pit depth and variance. However, they provide no justification for their choice of λ nor do they provide a physical interpretation for γ. Finally, the results in Figure 2 were obtained using the analytical solution Equation (9). We also obtained

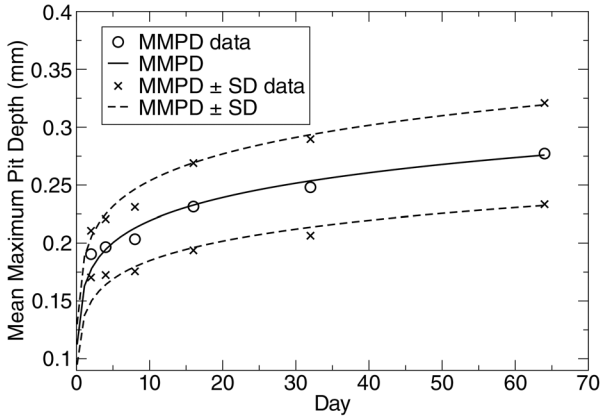

FIGURE 2. *Comparison of mean maximum pit depth (MMPD) and variance (standard deviation [SD]) computed by the MCP procedure with experimental data from.[12-13]*

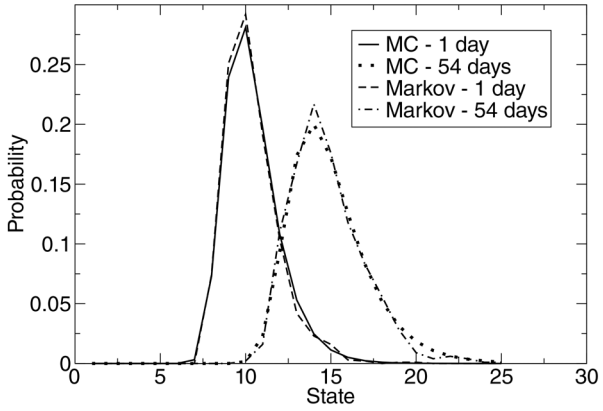

FIGURE 3. *Comparison of Monte Carlo (MC) and Markov chain process results for the probability mass function for the maximum pit depth. The model input parameters are the same as those used to generate Figure 2.*

solutions using numerical simulations of Equation (3) for the same data inputs as listed above. The analytical and numerical solutions were practically identical.

Figure 3 shows a comparison of results from the Monte Carlo and Markov chain process simulations for the probability mass function for the maximum pit depth. The excellent agreement between the two approaches provides some verification that the simplifications made in the cumulative distribution function, Equation (19), lead to reasonable results.

Benchmark the Model Against Long-Term Atmospheric Exposure Data

We present the use of the combined pit initiation/pit growth model to simulate pit initiation and the frequency distribution of pit depth where the metal is exposed to time-varying environmental conditions. Elola, et al.,[5] conducted field observations over 48 months where aluminum alloy (AA)1050 (UNS A91050) panels were exposed to the atmosphere for 1, 1.5, 3, 6, 13, 24, 36, and 48 months at different sites. Climate and level of pollutants varied over time at each location. For example, Figure 4 displays measured levels of surface-active sulfur at one of the exposure sites. In general, Elola, et al.,[5] state that pollutant and salinity levels tended to decrease over time for the 48 months of exposure. Hence, we assume that corrosive conditions changed from more aggressive to less aggressive states over this time period. We now illustrate the use of the Markov model to simulate this dynamic change in corrosive conditions. Both MC and MCP are conducted. However, different forms of λ_i are used in each simulation to contrast results based upon the choice of λ_i.

First, establish the pit initiation model. Data provided previously[5] suggest that the measured number of pits in the aluminum panels increased linearly over time for the 48-month period. Using Equations (1) and (2), we set A = 0 and β = 1 to simulate this linear behavior of the number of pits with time. The parameter ν is chosen based on a curve fit with the number of pit density data from Elola, et al.[5] Figure 5 shows a comparison between the data and the curve fit.

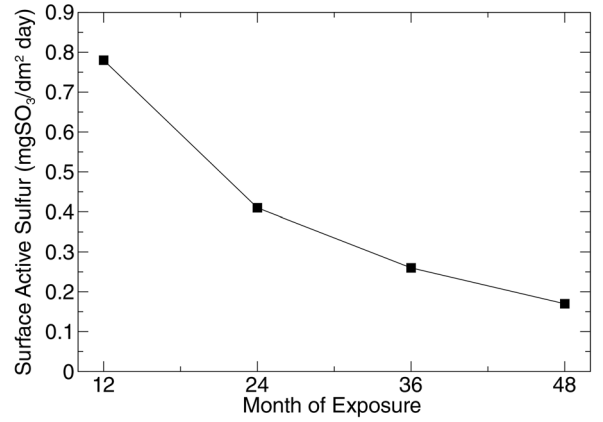

FIGURE 4. *Measured levels of surface active sulfur over time at an exposure site.*

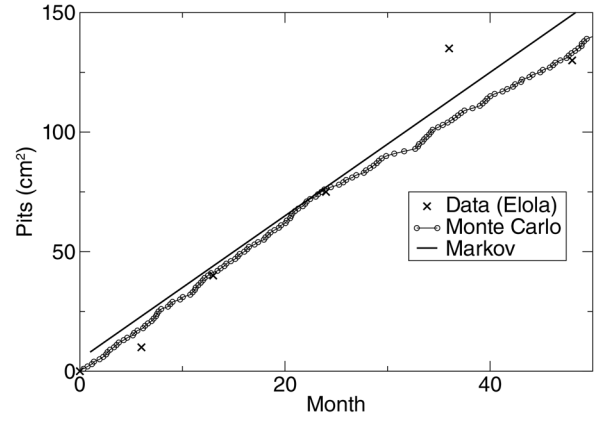

FIGURE 5. *Comparison of model computations of pit density with experimental observations.*

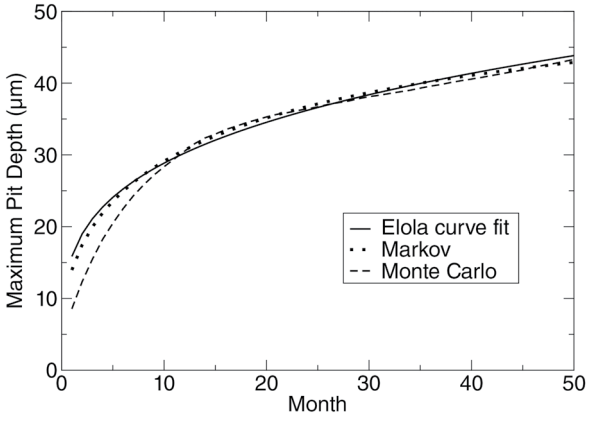

FIGURE 6. *Comparison of the mean maximum pit depth of the Elola, et al.,[5] curve fit to the data, with results computed by Monte Carlo simulations and Markov chain solutions for different values of the transition rate λ_i.*

Next, we establish the pit growth model. Based on the decrease in corrosive conditions over time, discussed in Figure 4, we propose the pit depth model $at^{b(t)}$, where $b(t) = \frac{1}{c_1 + c_2 t}$. This functional form imitates the sub-linear decrease in time seen in the figure. Using the curve fit for the mean maximum pit depth found in Elola, et al.,[5] as a guide (the curve fit was approximately $16t^{0.26}$), we propose using Equation (8) in the form $\lambda_{ai} = \frac{20}{i^{\frac{1-b}{b}}}$, where $b(t) = \frac{1}{\min\left(3+\frac{2.5t}{48}, 4.1\right)}$, so that b(t) decreases from 0.33 to 0.244 over time. This drop in the value of b simulates the change from aggressive to less aggressive corrosive conditions and, hence, the decrease in the power law growth rate of the pit depth.

A comparison between the mean maximum pit depth computed by our MC and MCP approaches, and that computed by Elola, et al.,[5] is shown in Figure 6. Here, we used the λ_{ai} expression described above in the MC simulations, and $\lambda_{bi} = \frac{b}{t - u + \epsilon}$. i with b = 0.229 and ϵ = 0.007729 in the MCP solutions. The different choices for the definition of λ_i were made because the latter fits the format allowing for use of the analytical Equation (9) while the former does not. Furthermore, the former model was designed to capture more of the dynamic changes in the environmental conditions than the latter.

Figure 6 shows that the MCP results (with λ_{bi}) for mean maximum pit depth agree with Elola, et al., over all time, while the MC results (with λ_{ai}) agree with Elola, et al., for long-term data, but differ in the short time. The Monte Carlo short-term results follow the power law $5.51t^{0.33}$, while the Elola model follows $16t^{0.26}$. Even though we have a larger power law exponent, 0.33, the smaller value, a = 5.51, puts our predicted curve below Elola, et al., for the short term. Nevertheless, all three curves for mean maximum pit depth show relatively the same results.

On the other hand, Figure 7 displays a comparison of the pit depth distribution measured by Elola, et al., against predictions from the Monte Carlo ($\lambda_{ai} = \frac{20}{i^{\frac{1-b}{b}}}$, where $b(t) = \frac{1}{\min\left(3+\frac{2.5t}{48}, 4.1\right)}$ procedure and the Markov chain ($\lambda_{bi} = \frac{b}{t - u + \epsilon}$i with b = 0.229 and ϵ = 0.007729) procedure. Clearly, the λ_{ai} model used in the Monte Carlo simulation provides a more accurate representation of the pitting corrosion occurring in this atmospheric exposure case than the λ_{bi} model used in the Markov chain simulation, even though both models gave reasonable predictions for the mean maximum pit depth. Hence, different pit depth distributions

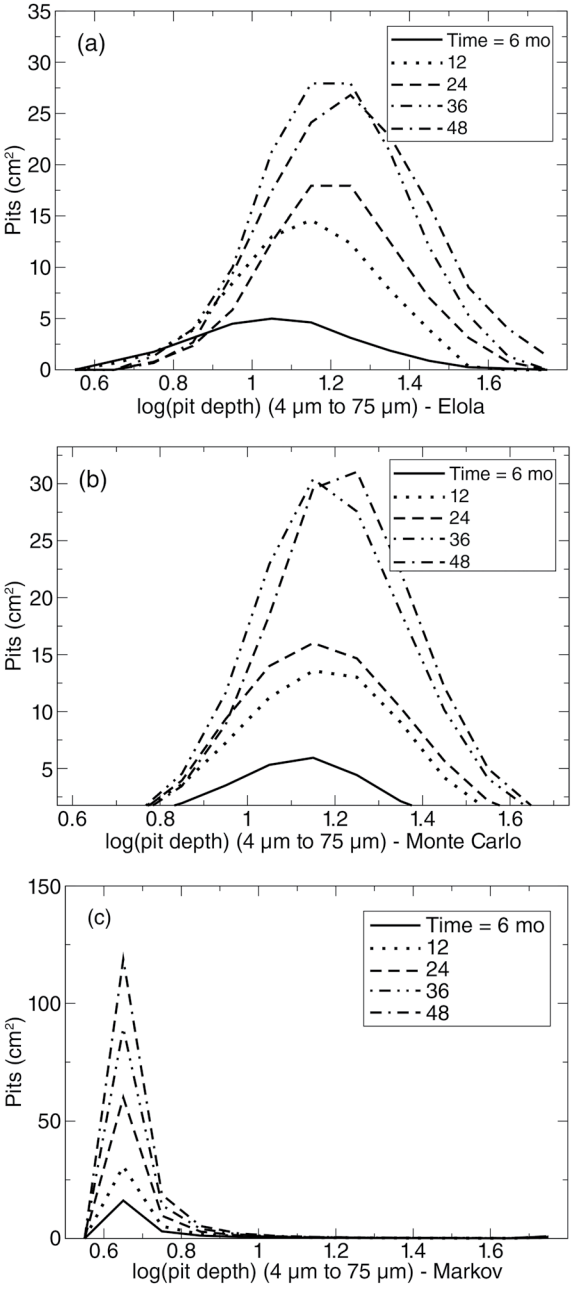

FIGURE 7. *Comparison of experimental pit depth distribution (a) over time[5] to pit depth distributions computed by Monte Carlo simulations, (b) Markov chain solutions, and (c) for different values of the transition rate λ_i.*

could lead to identical mean maximum pit depth distributions. Therefore, model predictions need to be benchmarked against additional pit depth measurements (beyond just mean maximum pit depth) to verify that the model is reasonably capturing all pit depth statistics. Further, Figure 7 illustrates that the proposed dynamic model for λ_i is able to provide reasonably accurate predictions of the pit depth distribution over the entire 48-month exposure period. This capability can be used in a probabilistic corrosion risk model to determine a risk value for the condition that pit depth is between prescribed depths.

Application of the Model to Simulate Hypothetical Pipeline Corrosion Scenarios for Internal Pitting Corrosion

Details for the following discussion are found elsewhere.[33] The discussion of the Elola, et al.,[5] data above illustrates the ability of the proposed Markov models to simulate corrosion in time-varying conditions. Given this capability we examine hypothetical internal pitting pipeline corrosion scenarios, using MCP solutions, to determine the probability of failure corresponding to the development of a leak in a pipe of given thickness (1-in [25.4-mm] thick steel pipe in the examples that follow). We develop a baseline corrosion situation (constant corrosive conditions over time) for the pipe. We discuss a variety of changes to the baseline case in response to several hypothetical scenarios:

—uncertainty in the number of pits
—a sudden increase in aggressiveness of the corrosive conditions
—a gradual increase in corrosive conditions
—episodic changes in conditions

For example, we compare responses to increasing carbon dioxide (CO_2) content in the production environment, causing a gradual increase in corrosive conditions, vs. an episodic event (water slug or failure of inhibitor injection), causing rapid changes in corrosive conditions over a short period of time. Additional scenarios are discussed elsewhere.[33] For example, modification of transition rates λ in time, as a result of information from in-line inspection data, is discussed. These hypothetical scenarios illustrate the flexibility of the proposed model to simulate varying operational conditions, as well as to accommodate adjustments due to availability of inspection data.

Given that data may not be available for pit density within a pipe, we pose several hypothetical pit initiation profiles (using Equation [1]) shown in Figure 8. The 50 pits/year model (A = 0, β = 1, and ν = 50) and the exponential initiation model (A = 7500, μ = 0.2, and ν = 0) were chosen to arrive at the same number of pits per area after 30 years, even though the pits nucleate at different rates. For discussions that follow, the baseline pit initiation rate will be the linear 50 pits/year case.

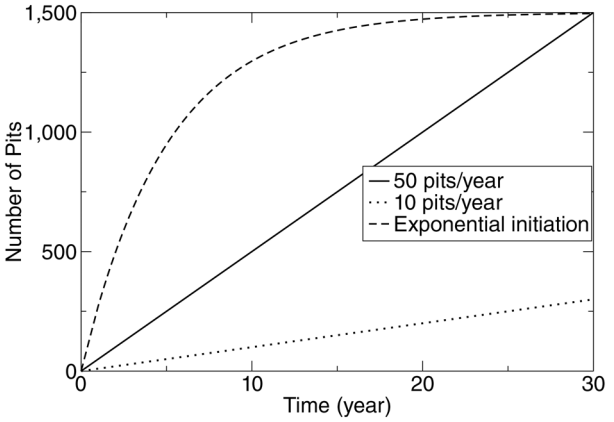

FIGURE 8. *Hypothetical pit initiation rates.*

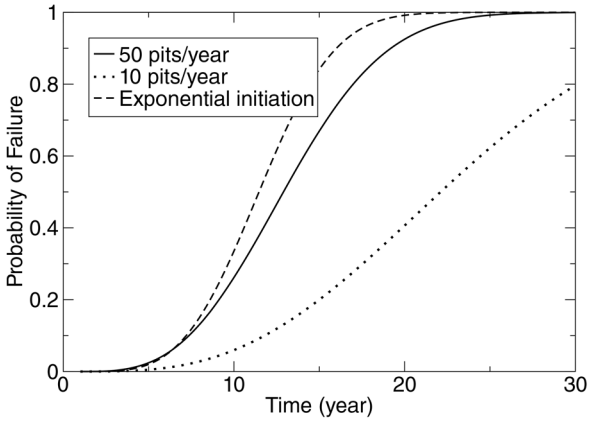

FIGURE 9. *Hypothetical pit initiation rate—constant corrosive conditions (b = 0.33): influence on the probability of failure defined as corrosion through a 1-in-thick pipe.*

As a baseline corrosion situation, we assume constant corrosive conditions over time, modeled by the choice b = 0.33. We also assume that the 1-in-thick pipe wall is discretized into n = 100 depth-of-damage states. Figure 9 shows the probability of failure, $1 - \theta_n(t)$, given the pit initiation rates displayed in Figure 8. As expected for fewer pits, the probability of failure is smaller. Further, for the same number of pits after 30 years, the exponential pit initiation rate yields a greater likelihood of failure because the pits nucleate sooner and can grow more.

In Figure 10, we present the probability of being in damage states 20, 50, or 90, which correspond to a pit that is about 0.2 in (5.1 mm), 0.5 in (12.7 mm) or 0.9 in (22.9 mm) in depth. As discussed above, the probability of being in a state decreases with fewer pits as shown in this figure. Predictions of the probability of being in a particular state may be relevant to defining maintenance schedules or defining a working definition of failure.

One of the input parameters to the model is the number of states used in the discretization of the 1-in-thick pipe. The choice for the number of states

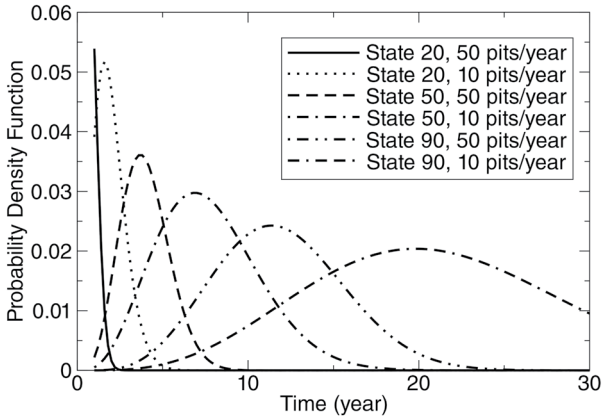

FIGURE 10. *Probability density function for being in states 20, 50, or 90 using the same hypothetical parameter inputs as in Figure 9.*

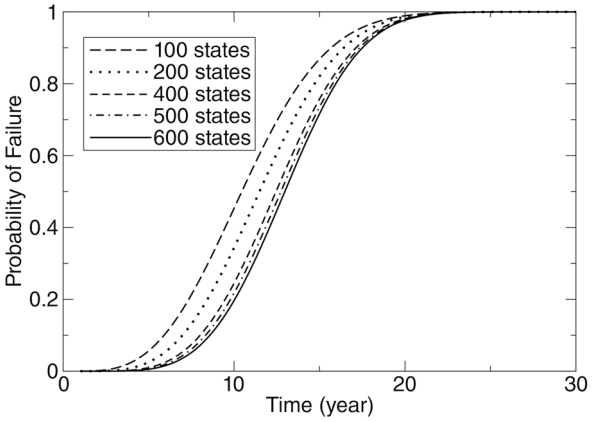

FIGURE 11. *Sensitivity of the probability of failure to the number of states in the Markov model. Here, the probability of transition from state to state, λ_i, is a function of the number of states.*

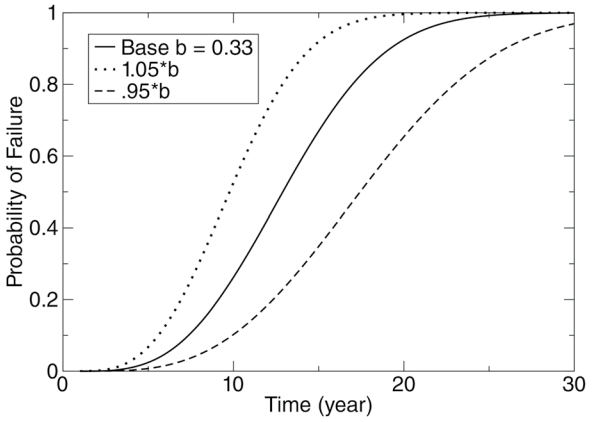

FIGURE 12. *Sensitivity of the probability of failure to a 5% change in the transition rate between states. The same hypothetical parameter inputs as in Figure 9 are used.*

will depend upon the accuracy desired for the pit depth. For example, if one wants to know when the pit depth is within a prescribed depth tolerance, then the tolerance will determine the length, C, of the discretized states. To examine the influence of the number of states on the results, Figure 11 shows the predicted probability of failure as the number of states used in the discretization of the 1-in-thick pipe increases. As the number of states increases, the value for b also increases. This follows since it is necessarily quicker to reach the next state because of the smaller incremental depth of damage between states. This is consistent with λ_i increasing with the decrease in incremental depth according to Equation (8). As a general rule of thumb we find that if one benchmarks the parameter b for a given state width C (say a large value of C leading to a coarse discretization into n_{coarse} states), then λ_i is adjusted according to:

$$\lambda_{fine} = \left(1 + b \ln\left(\frac{n_{fine}}{n_{coarse}}\right)\right)\lambda_{coarse} \qquad (23)$$

as one moves to a finer mesh with a larger 557 number of states, n_{fine}. In other words, the parameters, such as b, are calibrated once for the data set after C is chosen. The parameters do not need to be recalculated if one chooses to adjust the number of states. Rather, the rule of thumb allows one to only adjust the original value of λ_i. This rule of thumb expression was derived through trial and error. The logarithmic form of the rule appears reasonable given the exponential form of solutions, Equation (9), for the MCP method. The above discussion on the number of states is relevant to the calibration of the model. Any baseline configuration of parameters chosen to represent a specified corrosion situation is necessarily dependent upon values for both b and C.

Figure 12 shows the sensitivity of the probability of failure to slight changes (5%) in the value of b. For this particular scenario there is about a 5 year discrepancy in the predicted time to failure as a result of the proposed uncertainty in the value of b. Here, predicted time to failure is the time at which the probability of failure is 50%.

Next, we examine three hypothetical scenarios for changes in corrosive conditions during the operation of the pipe. First, we consider the effect of a sudden increase in the aggressiveness of corrosion at year 8 of operation of the pipeline. This might be because of a loss of inhibitor effectiveness or a sudden increase in chlorides. We model the increase in corrosion by a step change increase in the value of b at year 8, as shown in Figure 13. As anticipated, the probability of failure increases as a result of the change.

In Figure 14, we examine the effects of a gradual increase (in this case a linear increase) in corrosive conditions over time. This might be because of watercut or souring. Again, as the aggressiveness of the corrosive conditions increase, the probability of failure also increases.

Finally, we simulate an episodic increase in corrosive conditions as a result of a water slug or inhibi-

tor injection failure. We assume the incident occurs at either year 3 or year 8 and lasts for 3 months until it is corrected (b increases to 1.25b for 3 months and then returns to b). For the values of b chosen for this simulation, Figure 15 shows there is a slight increase in the probability of failure because of the episode.

CONCLUSIONS

We developed and demonstrated Markov process probabilistic analysis tools for corrosion risk management capable of accounting for corrosion under dynamic changes in environmental conditions. Specifically, we used both MC simulations and MCP solution procedures to simulate combined pit initiation and pit growth. The MCP approach offers the advantage of faster computational times. These Markov models are developed to compute pitting damage accumulation density distributions as a function of input parameters for the pit nucleation and growth rates. The input parameters are selected based on comparison with experimental or field observations over a sufficient period of time. An advantage of the proposed models is that the input parameters are related to familiar corrosion concepts, such as exponential or linear pit initiation profiles, and power law models for pit depth. Hence, selection of the parameters may be intuitive.

Our proposed model combines a nonhomogeneous Poisson process for pit initiation with a Markov process for pit growth. The Markov process is capable of including any form of the pit state probabilistic transition rate, $\lambda_i(t)$. Further, combined model calculations for the cumulative distribution function, $\theta_i(t)$, for the probability that the maximum pit depth is less than or equal to state i, may be calculated using the complete Equation (12), in the form of Equation (17), through MC simulations, or calculated using the simplified expression, Equation (19), through MCP solutions. We show a comparison of the two results in the "Results and Discussion" section. The excellent agreement between the two results justifies use of the simplified expression.

The proposed model is similar to other Markov models for pitting corrosion,[12-20] but differs in its pit initiation model, as well as the proposed transition rate, λ_i. For example, Hong[15] successfully combined pit initiation processes with the Markov pit growth model, but the initiation process was modeled by a homogeneous Poisson process, and λ_i was taken to be the same constant for all states i. Valor, Caleyo, and others[16-17,20] have mentioned the nonhomogeneous Poisson process as a candidate for the pit initiation process but chose to use the Weibull distribution. Also, their Markov process was restricted to the form $\lambda_i(t) = \alpha(t)i$. Finally, none of the research[12-20] presented earlier detailed a means to calculate the cumulative distribution function, Equation (12), for the probabil-

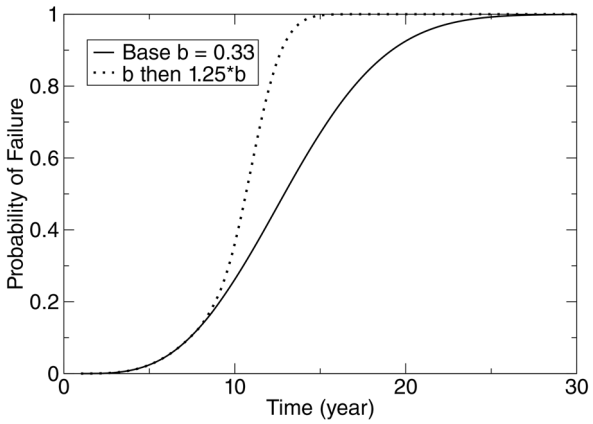

FIGURE 13. *Example of a sudden increase in corrosive conditions as a result of a loss of inhibitor effectiveness (in year 8) as modeled by a step change increase in the transition rate. The same hypothetical parameter inputs as in Figure 9 are used.*

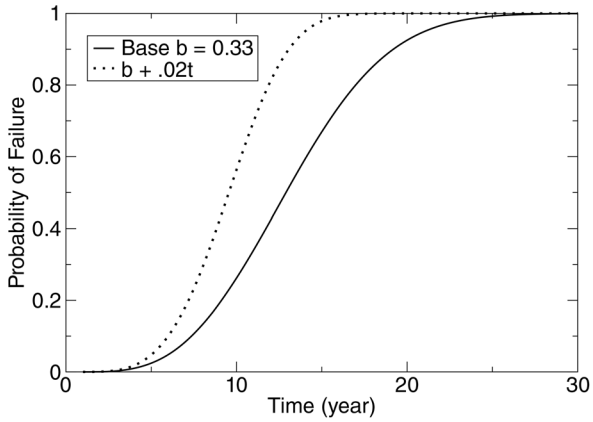

FIGURE 14. *An example of gradual increase in corrosive conditions as a result of water-cut or souring as modeled by a linear change in transition rate. The same hypothetical parameter inputs as in Figure 9 are used.*

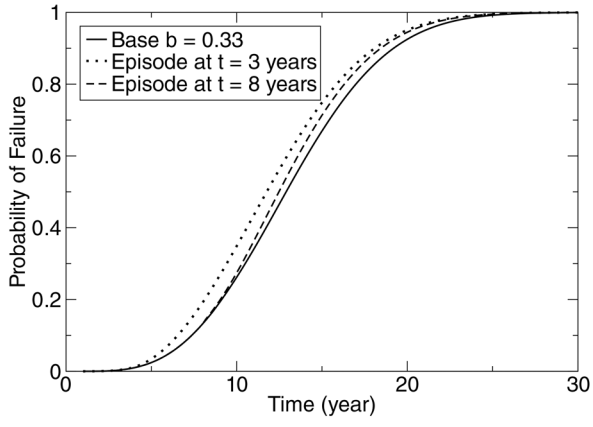

FIGURE 15. *Example of an episodic increase in corrosive conditions (at either year 3 or year 8) from a water slug or inhibitor injection failure, modeled by a step change increase to b = 0.4125 in transition rate for 3 months followed by return to normal b = 0.33. The same hypothetical parameter inputs as in Figure 9 are used.*

ity that the maximum pit depth is less than or equal to state i, from the combined pit initiation/Markov pit growth process as presented here. Therefore, to the best of our knowledge, this is the first manuscript that offers a detailed calculation of the maximum pit depth distribution using combined nonhomogeneous Poisson and Markov processes. Our final product is Equation (19) that allows for fast calculation of $\theta_i(t)$ without any restriction on $\lambda_i(t)$.

To implement the procedures in a corrosion risk management program, one should complete the following:

❖ Decide on the number of states needed based upon the level of accuracy required for determination of the pit depth. For example, if a critical pit depth has been identified, as well as the accepted tolerance levels around this critical depth, then the width of states should be less than or equal to the tolerance level. If the number of states needs to be changed, then Equation (23) provides a guide for adjusting the pit transition rate between depth states.

❖ Gather data on the distribution of pit density over time and use this information to select parameters in the definitions, Equations (1) and (2), of the pit nucleation model to fit the data. Equation (1) provides an intuitive model, using basic functions, for choosing the fitting parameters.

❖ Gather data on the pit depth distribution or pit growth rate over time and use this information to select parameters in the definition of the pit transition rate between depth states (Equation [6] or [8]) to fit the data. Parameters in these equations were shown to have an intuitive connection to power law models for the pit depth.

❖ Calculate the cumulative probability distribution of being less than a particular depth state over time using MC with Equation (12) in the form, Equation (17), or MCP with Equation (19), and the pit nucleation and pit growth rate laws defined in the preceding items.

❖ Compute a variety of damage accumulation statistics such as mean maximum pit depth and its variance over time, pit depth distributions over time, and probability of corroding to a prescribed critical depth over time, using the cumulative probability distribution.

❖ Modify pit nucleation and pit growth rate parameters to simulate changes in environmental conditions to examine hypothetical corrosion scenarios.

Both MC and MCP computations for pit depth distribution were benchmarked against laboratory pitting corrosion tests and against long-term atmospheric exposure data. In the latter case we demonstrated the capabilities of the models to account for corrosion under time-varying environmental conditions.

Since the input parameters to the models are selected upon characterization with experimental or field observations over a sufficient period of time, future work will fit parameters for a number of different materials in varying environmental conditions, to validate the robustness of the models. Ultimately, we envision the development of an interactive tool whereby the user adjusts slider bars to set the input parameters and establish the baseline corrosion situation. Once agreement with baseline data is achieved, then hypothetical situations may be investigated to make risk assessment and maintenance decisions. For example, we examined an internal pitting pipeline corrosion scenario and determined the probability of failure corresponding to development of a leak. We developed a baseline corrosion situation (constant corrosive conditions over time) for a steel pipe. We discussed a variety of changes to the baseline case in response to several hypothetical scenarios:

—a sudden increase in corrosive conditions
—a gradual increase in corrosive conditions
—episodic changes in conditions

These hypothetical scenarios illustrate the flexibility of the model to simulate varying operational conditions, as well as to accommodate adjustments due to availability of inspection data.

ACKNOWLEDGMENTS

This work is associated with the National Corrosion Center (NCERCAMP–National Center for Education and Research on Corrosion and Materials Performance) at The University of Akron and the DoD Technical Corrosion Collaboration supported by the U.S. Department of Defense Office of Corrosion Policy and Oversight through the Engineering Research and Development Center/U.S. Army Construction Engineering Research Laboratory Grant W9132T-11-0002, and through the U.S. Air Force Academy under agreement number FA7000-10-2-0013. The authors thank D.J. Dunmire and R. Hays for their continued support.

REFERENCES

1. R.P. Wei, *Scr. Mater.* 44, 11 (2001): p. 2647-2652.
2. D.E. Williams, C. Wescott, M. Fleischmann, *J. Electrochem. Soc.* 132 (1985): p. 1796-1804.
3. D.E. Williams, C. Wescott, M. Fleischmann, J. Electrochem. Soc. 132 (1985): p. 1804-1811.
4. J.R. Galvele, *J. Electrochem. Soc.* 123, 4 (1976): p. 464-474.
5. A.S. Elola, T.F. Otero, A. Porro, *Corrosion* 48, 10 (1992): p. 854-863.
6. S.T. Pride, J.R. Scully, J.L. Hudson, *J. Electrochem. Soc.* 141, 11 (1994): p. 3028-3040.
7. M.K. Cavanaugh, N. Birbilis, R.G. Buchheit, *Electrochim. Acta* 59 (2012): p. 336-345.
8. G.S. Frankel, *J. Electrochem. Soc.* 145, 6 (1998): p. 2186-2198.
9. D.G. Harlow, R.P. Wei, *Eng. Fract. Mech.* 59, 3 (1998): p. 305-325.
10. D.G. Harlow, R.P. Wei, *Fatigue Fract. Eng. Mater. Struct.* 22, 5 (1999): p. 427-436.
11. M.K. Cavanaugh, R.G. Buchheit, N. Birbilis, *Eng. Fract. Mech.* 76, 5 (2009): p. 641-650.
12. E.S. Rodriguez, III, J.W. Provan, *Corrosion* 45, 3 (1989): p. 193-206.
13. J.W. Provan, E.S. Rodriguez, III, *Corrosion* 45, 3 (1989): p. 178-192.
14. T. Shibata, *Corrosion* 52, 11 (1996): p. 813-830.

15. H.P. Hong, *Corrosion* 55, 1 (1999): p. 10-16.
16. A. Valor, F. Caleyo, L. Alfonso, D. Rivas, J.M. Hallen, *Corros. Sci.* 49 (2007): p. 559-579.
17. F. Caleyo, J.C. Velazquez, A. Valor, J.M. Hallen, *Corros. Sci.* 51 (2009): p. 2197-2207.
18. L.V. Poluyan, A.V. Bushinskaya, M.G. Malyukova, S.A. Timashev, "Reliability-Based Inspection and Maintenance of Pipelines with Markov Type Corrosion Defects Growth," in *Safety, Reliability and Risk of Structures, Infrastructures and Engineering Systems*, paper no. ICOSSRO9-0156 (Boca Raton, FL: CRC Press, 2010), p. 4001-4008.
19. A.V. Bushinskaya, S.A. Timashev, *J. Mach. Manuf. Reliab.* 39, 5 (2010): p. 504-510.
20. A. Valor, F. Caleyo, L. Alfonso, J.C. Velazquez, J.M. Hallen, *Math. Prob. Eng.* (2013): p. 1-13.
21. B. Wu, J.R. Scully, J.L. Hudson, A.S. Mikhailov, *J. Electrochem. Soc.* 144, 5 (1997): p. 1614-1619.
22. T.T. Lunt, S.T. Pride, J.R. Scully, J.L. Hudson, A.S. Mikhailov, *J. Electrochem. Soc.* 144, 5 (1997): p. 1620-1629.
23. T.T. Lunt, J.R. Scully, V. Brusamarello, A.S. Mikhailov, J.L. Hudson, *J. Electrochem. Soc.* 149 5 (2002): p. B163-B173.
24. N.D. Budiansky, L. Organ, J.L. Hudson, J.R. Scully, *J. Electrochem. Soc.* 152 4 (2002): p. B152-B160.
25. L. Organ, J.R. Scully, A.S. Mikhailov, J.L. Hudson, *Electrochim. Acta.* 51 (2005): p. 225-241.
26. A.S. Mikhailov, J.R. Scully, J.L. Hudson, *Surf. Sci.* 603 (2009): p. 1912-1921.
27. N. Murer, R.G. Buchheit, *Corros. Sci.* 69 (2013): p. 139-148.
28. R.E. Melchers, *Corrosion* 61, 7 (2005): p. 655-664.
29. R.E. Melchers, *Corrosion* 61, 8 (2005): p. 766-777.
30. E. Parzen, *SIAM Rev.* 5, 2 (1999): p. 172-173.
31. A. Prados, J.J. Brey, B. Sańchez-Rey, *J. Stat. Phys.* 89, 3/4 (1997): p. 1-13.
32. J. Zhao, "Probabilistic Analysis of Reliability Using Markov Processes" (Master's thesis, The University of Akron, 2014).
33. K.A. McCallum, "Probabilistic Analysis of Pipeline Reliability Using a Markov Process" (Master's thesis, The University of Akron, 2012).